

First Multi-Constellation Observations of Navigation Satellite Signals in the Lunar Domain by Post-Processing L1/L5 IQ Snapshots

LORENZO SCIACCA , Graduate Student Member, IEEE
 ALEX MINETTO , Member, IEEE
 ANDREA NARDIN , Member, IEEE
 FABIO DOVIS , Member, IEEE
 Politecnico di Torino, Turin, Italy

LUCA CANZIAN
 Qascom Srl, Cassola, Italy

MARIO MUSMECI
 CLAUDIA FACCHINETTI
 GIANCARLO VARACALLI
 Agenzia Spaziale Italiana, Rome, Italy

Abstract—

The use of Global Navigation Satellite Systems (GNSS) to increase spacecraft autonomy for orbit determination has gained renewed momentum following the Lunar GNSS Receiver Experiment (LuGRE), which demonstrated feasible onboard GPS and Galileo signal reception and tracking at lunar distances. This work processes in-phase and quadrature (IQ) snapshots collected by the LuGRE receiver in cis-lunar space and on the lunar surface to assess multi-frequency, multi-constellation signal availability. Signals from additional systems beyond GPS and Galileo, including RNSS and SBAS constellations, are observable and successfully acquired exclusively in the recorded IQ snapshots. These observations provide the first experimental evidence that signals from multiple constellations—including systems not supported by LuGRE real-time operations—are detectable at unprecedented distances from Earth. Useful observables can be extracted from the IQ snapshots,

Manuscript received XXXXX 00, 0000; revised XXXXX 00, 0000; accepted XXXXX 00, 0000.

DOI. No. XXXXX

Refereeing of this contribution was handled by XXXX XXXX. This study was funded within the contract n. 2021-26-HH.0 between Agenzia Spaziale Italiana and Politecnico di Torino "Attività di Ricerca e Sviluppo inerente alla Navigazione GNSS nello Space volume Terra/Luna nell'ambito del Lunar GNSS Receiver Experiment". This publication is also part of the project PNRR-NGEU which has received funding from the MUR – DM 630/2024.

Authors' addresses: Lorenzo Sciacca, Alex Minetto, Andrea Nardin, Fabio Dovis are with the Department of Electronics and Telecommunications, Politecnico di Torino, Turin, TO, 10124 Italy (e-mail: name.surname@polito.it); Luca Canzian is with Qascom Srl, Cassola, VI, 36022 Italy (e-mail: luca.canzian@qascom.it)

©2026 IEEE. Personal use of this material is permitted. Permission from IEEE must be obtained for all other republication or redistribution.

despite minimal sampling rates, 4-bit quantization, and short durations (200 ms–2 s), through a hybrid coherent/non-coherent acquisition stage compensating for code Doppler. These observations are exploited to tune simulation tools and to perform extended simulation campaigns, showing that the inclusion of additional constellations significantly improves availability; for a 26 dB-Hz acquisition threshold, the fraction of epochs with at least four visible satellites increases from 11% to 46% of the total epoch count. These findings indicate that BeiDou, RNSS, and SBAS signals can substantially enhance GNSS-based autonomy for lunar and cis-lunar missions.

Index Terms— deep-space GNSS, Global Navigation Satellite Systems (GNSS), lunar navigation, regional navigation satellite systems (RNSS), signal acquisition, space-based augmentation systems (SBAS), space exploration

I. Introduction

As mission designs grow more complex and the number of planned lunar missions increases [1], the demand for navigation solutions that provide greater onboard autonomy in orbit determination and can scale with future mission needs has become a practical and strategic necessity. Historically, spacecraft operating beyond Earth orbit have depended primarily on ground-based Radio Frequency (RF) tracking networks, such as Deep Space Network (DSN), European Space Tracking Network (ESTRACK), ISRO Telemetry, Tracking and Command Network (ISTRAC), and Chinese Deep Space Network (CDSN) to support navigation, guidance, and maneuvering. In parallel, recent progress in lunar exploration has highlighted the potential of Global Navigation Satellite System (GNSS) as a complementary resource for navigation in the lunar domain, encompassing cis-lunar space and the lunar surface, making the exploitation of these signals an increasingly compelling complement [2].

In particular, the Lunar GNSS Receiver Experiment (LuGRE) [3], [4] — a joint NASA–ASI experiment hosted on Firefly Aerospace Inc.'s Blue Ghost Mission 1 (BGM1) lunar lander under NASA's Commercial Lunar Payload Services (CLPS) program — was designed to acquire and track Global Positioning System (GPS) and Galileo signals in the L1/E1 and L5/E5a frequency bands along its trajectory to the Moon and during lunar surface operations, thereby exploiting the resulting observables to estimate the onboard receiver state, i.e., computing its Position, Velocity, Time (PVT). Launched in January 2025, LuGRE achieved historic milestones, including multiple GNSS-only PVT fixes along its trajectory and the first GNSS-only position fix on the lunar surface [2].

Beyond computing onboard PVT solutions, the LuGRE payload [5], [6] collected more than 106 hours of unprecedented raw GNSS observables, as well as approximately 12 s of In-phase and Quadrature Samples (IQS) snapshots, with snapshot durations ranging from 200 ms to 2 s, collected across different operational windows. As a result, the openly available LuGRE dataset [7] provides, in addition to state-estimation solutions, both IQS snapshots and GNSS receiver observables collected throughout the mission.

TABLE I

List of constellations transmitting SBAS signals (source: International GNSS Service (IGS)).

System	Number of satellites
AI-SBAS	1
BDSBAS	3
EGNOS	3
GAGAN	3
KASS	2
MSAS	2
NSAS	1
Pak-SBAS	1
QZSS	5
SouthPAN	1
SDCM	3
WAAS	3

This paper leverages the unique IQS snapshots obtained by LuGRE [3], [4], to demonstrate the availability of additional navigation signals from systems not originally exploited during mission operations, i.e., BeiDou, the Quasi-Zenith Satellite System (QZSS), the Indian Regional Navigation Satellite System (IRNSS) (also known as NavIC) and Satellite-based Augmentation System (SBAS) constellations. A list of the constellations transmitting SBAS signals is reported in Table I.

Beyond the experimental demonstration itself, the information extracted from the openly available IQS snapshots [7] is used to calibrate and validate an advanced extended Space Service Volume (SSV) simulator. This calibration, grounded directly on in-space experimental data, enables realistic simulation of LuGRE operations while explicitly accounting for the contribution of additional GNSS, Regional Navigation Satellite System (RNSS), and SBAS constellations not processed during LuGRE operations. As a result, the simulator provides, for the first time, an experimentally anchored assessment of multi-constellation signal availability in the cis-lunar and lunar environments.

The remainder of the article is organized as follows. Section II describes the relevant features of the LuGRE payload and Sample Capture (SC) operations. Section III describes the acquisition stage utilized for processing snapshots of IQS and the extended SSV simulator employed to assess the experimental outcomes. Section IV analyzes acquisition results and multi-frequency, multi-constellation signal availability, while Section V provides the conclusions.

II. Background

Several experiments have demonstrated the feasibility of using GNSS signals beyond Low Earth Orbit (LEO). Notably, National Aeronautics and Space Administration (NASA)'s Magnetospheric Multiscale (MMS) mission exploited GPS signals at distances of up to approximately 50% of the Earth–Moon distance [8], [9], [10]. Complementarily, the Canadian Advanced Nanosatellite

eXperiment-2 (CanX-2) mission demonstrated SBAS-based ranging in LEO [11], [12], revealing the need for dedicated corrections to mitigate residual clock offsets on the order of 100 m and for ephemerides more accurate than those provided by the SBAS Satellite Vehicles (SVs). The missions discussed above did not lead to the release of publicly available datasets in the form of signal samples. The LuGRE mission, instead, provides openly accessible data [7]. Accordingly, this section presents an overview of LuGRE, with particular emphasis on the LuGRE payload and the IQS data collection operations.

A. The LuGRE Payload

The LuGRE payload consisted of the Qascom QN400-SPACE (QN400-S) receiver, together with a dedicated High Gain Antenna (HGA), a Low Noise Amplifier (LNA), and the harnesses required to connect all components. The receiver includes two independent boards controlled by a supervisory module to ensure complete redundancy. For most of the mission, the primary board handled all operations, while the secondary board was used only during the final two operations.

The payload's HGA was specifically designed for the reception of GNSS signals in the L1/E1 and L5/E5a bands. It provides a peak boresight gain of 15.35 dBic and includes an integrated notch filter to suppress out-of-band interference. During the transit phase operations, the antenna, mounted on a gimbaled platform, was kept pointed toward the Earth by adjusting the spacecraft attitude while keeping the gimbal fixed, resulting in an Earth-Off-Pointing angle consistently below the nominal limit of 1°. During the surface phase, the active gimbal steering further improved alignment, achieving Earth-Off-Pointing angles better than 0.21° [2]. Consequently, antenna pointing error can be neglected for the analysis conducted in this work.

The LuGRE payload was integrated into the BGM1 lander as a scientific instrument and operated in full compliance with strict do-no-harm requirements [2], [6]. The lander did not rely on the payload for any spacecraft maneuvers, as the receiver was not interfaced with the Guidance Navigation and Control (GNC) system.

The QN400-S receiver supports a Real-Time Processing (RTP) mode in which it autonomously handles signal acquisition, tracking, and state estimation using GPS and Galileo signals in the L1/E1 and L5/E5a bands. At scheduled intervals, the receiver was configured in SC mode, during which the receiver's front end collected raw IQS snapshots on the same bands for subsequent downlink.

The receiver provided multiple Analog to Digital Converter (ADC) configurations to serve for SC mode. During standard RTP operations, sampling was performed at 24 Msps with 16-bit quantization. For L1/E1 acquisition, samples were decimated to 6 Msps (16-bit), while the L5/E5a acquisition uses the full 24 Msps (16-bit). During

tracking, L1/E1 signals are processed at 12 Msps (16-bit), while L5/E5a continues at 24 Msps (16-bit).

The IQS snapshots collected in SC mode were sampled at frequencies between 4 MHz and 24 MHz, with 4-bit or 8-bit quantization. Due to the limited downlink bandwidth shared among all payloads and subsystems, sampling and quantization choices directly impacted the available snapshot duration, limiting each snapshot to a maximum of two seconds, and higher-fidelity sampling configurations could not be used [13]. Although the SC and RTP modes were mutually exclusive, the two modes were frequently executed in succession within the same operational window. Detailed timing, sequencing, and duration of these mode transitions for each operation are documented in the LuGRE operations summary table (OPTABLE) contained in the mission’s public dataset [7] and in [2].

B. LuGRE Sample Capture Operations

The start time of each SC operation was selected to maximize the availability of GPS and Galileo signals, when possible. Satellite visibility forecasts used during mission planning were generated using the Goddard Enhanced Onboard Navigation System (GEONS) and GEONS Ground Matlab Simulation (GGMS) tools [2].

The present article examines only data originated by operations featuring a SC, and all results are obtained from the post-processing of the corresponding IQS snapshots. Table II summarizes these operations, indicating, for each one, the ADC configuration and the duration of the acquired signal snapshots. When both L1/E1 and L5/E5a IQS snapshots were collected, the reported duration refers to both bands. Only operations in which the receiver was configured in SC mode are listed. The table also provides the Coordinated Universal Time (UTC) start time of each SC operation, denoted as *SC start*, together with the associated Julian day (*DoY*). UTC timestamps assigned by the onboard computer to SC operations, along with additional receiver status information, are available in the publicly released dataset [7].

Fig. 1 shows an example of the estimated Power Spectral Density (PSD) of the IQS snapshots for one of the possible ADC configurations on L1 band. As shown in [2], the spurious frequencies observed are not expected to affect the measurement quality discussed in this work. Nonetheless, all operations exhibit a significant frequency drift that is inconsistent with the expected receiver dynamics. For the sake of completeness, Fig. 2 presents the frequency drift relative to the start time of the SC operation for a representative set of cases, where the frequency offset is estimated over multiple IQS snapshot windows. The frequency offset drift is expected to affect the acquisition stage inducing a reduced performance by introducing a correlation loss dependent on the acquisition stage parameters. However, the RTP dataset is less affected by the drift [2], it is likely that the drift is introduced by the receiver clock when a reset

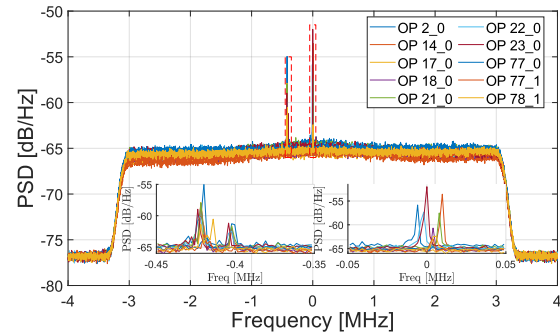


Fig. 1. Example of PSD obtained from the analysis of a subset of the IQS snapshots. Quantization: 4 bits; sampling frequency: 8 MHz; band: L1.

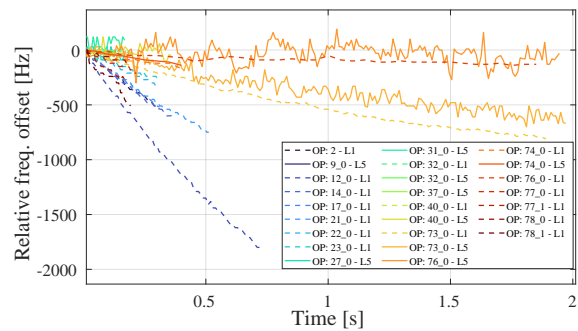


Fig. 2. Frequency offset drift, expressed relatively to the initial frequency offset, observed over the duration of each IQS snapshot. Only a subset of the collected snapshots is included.

of the receiver is performed, this happens when selecting the SC and at the RTP mode as well; anyway in RTP mode the receiver clock requires many seconds between the acquisition and the beginning of the signal tracking to stabilize itself. A further analysis on the root causes is out of scope and left for future works.

III. Methodology

A. Signal Acquisition Architecture and Methods

The adopted signal acquisition method is based on a hybrid coherent and non-coherent integration scheme with code Doppler compensation, as investigated in previous analyses [14]. For background on standard GNSS signal acquisition architectures and methods, the interested reader is referred to [15]. The set of acquisition parameters chosen for the acquisition of the GNSS, RNSS, and SBAS signals under analysis is provided in Table III. As reported in the literature [16], [17], [18], signal acquisition can be performed efficiently using a Discrete Fourier Transform (DFT)-based approach, which significantly reduces computational complexity. The mathematical formulation of the process is provided in the following, while a schematic representation of the Cross Ambiguity Function (CAF) computation and of the Carrier to Noise

TABLE II
Summary of LuGRE's SC operations.

Mission phase	OP identifier	DoY(2025)	SC start (UTC hh:mm:ss)	Snapshot duration [ms]	SC configuration	
Commissioning	2_0	16	01:31:11	400	4 bit, 8 MHz L1/E1	
	5_0	19	04:52:03	200	8 bit, 8 MHz L1/E1	
	9_0	25	05:08:14	200	4 bit, 24 MHz L5/E5	
	12_0	30	04:25:01	800	4 bit, 4 MHz L1/E1	
	Transit	14_0	30	22:40:47	400	4 bit, 8 MHz L1/E1
		17_0	34	09:13:32	400	4 bit, 8 MHz L1/E1
		18_0	36	22:59:01	600	4 bit, 8 MHz L1/E1
		21_0	38	23:29:01	600	4 bit, 8 MHz L1/E1
22_0	43	03:47:46	400	4 bit, 8 MHz L1/E1		
Lunar Orbit	23_0	45	04:58:44	400	4 bit, 8 MHz L1/E1	
	27_0	50	15:22:40	200	4 bit, 24 MHz L5/E5	
	31_0	54	03:40:08	200	4 bit, 24 MHz L5/E5	
	32_0	55	12:04:39	300	4 bit, 24 MHz L5/E5; 4 bit, 8 MHz L1/E1	
	37_0	58	16:09:27	300	4 bit, 24 MHz L5/E5; 4 bit, 8 MHz L1/E1	
Lunar Surface	38_0	62	06:12:50	300	4 bit, 24 MHz L5/E5; 4 bit, 8 MHz L1/E1	
	40_0	63	07:03:12	400	4 bit, 24 MHz L5/E5; 4 bit, 8 MHz L1/E1	
	73_0	73	10:09:35	2000	4 bit, 24 MHz L5/E5; 4 bit, 8 MHz L1/E1	
	74_0	73	12:47:07	500	4 bit, 24 MHz L5/E5; 4 bit, 8 MHz L1/E1	
	76_0	74	13:07:16	2000	4 bit, 24 MHz L5/E5; 4 bit, 8 MHz L1/E1	
	77_0	75	15:12:22	300	4 bit, 8 MHz L1/E1	
	77_1	75	19:14:55	300	4 bit, 8 MHz L1/E1	
	78_0	75	22:03:52	300	4 bit, 8 MHz L1/E1	
	78_1	75	22:11:20	300	4 bit, 8 MHz L1/E1	

Density Ratio (C/N_0) estimation process is reported in Fig. 3 [15]. Given the high dynamics of the scenario and the behavior of the payload clocks during operations, the Doppler effect and the receiver clock drift significantly affect the correlation between the received and locally generated codes [19], [20]. As a result, the code Doppler must be accounted for when generating the local carrier and the local code.

To implement the DFT-based acquisition scheme, the received signal $r[n]$ is multiplied by the local carrier testing for the frequency offset \tilde{f}_D obtaining

$$r_{\tilde{f}_D}[n] = r[n] \cdot e^{j2\pi(f_{IF} + \tilde{f}_D)\frac{n}{f_s}}, \forall n \in \{0, \dots, K \cdot N - 1\}, \quad (1)$$

where:

- f_{IF} is the intermediate frequency ($f_{IF} = 0$ for LuGRE SC operations),
- \tilde{f}_D is the frequency offset under test,
- f_s is the sampling frequency,
- K is the number of non-coherent accumulation,
- N is the number of samples in a coherent integration time $T_{coh} = N/f_s$.

The acquisition metric $S[\tilde{f}_D, \tau]$, for the frequency offset under test \tilde{f}_D is computed through a non-coherent integration of coherent correlation results, as detailed below. Specifically, the non-coherent integration is obtained

as

$$S[\tilde{f}_D, \tau] = \frac{1}{K} \sum_{j=0}^{K-1} S_j[\tilde{f}_D, \tau], \quad (2)$$

where

$$S_j[\tilde{f}_D, \tau] = Y_j[\tilde{f}_D, \tau] \cdot Y_j^*[\tilde{f}_D, \tau] \quad (3)$$

is the modulus-squared CAF computed over N -sample signal sequences. $Y_j[\tilde{f}_D, \tau]$ is evaluated as

$$Y_j[\tilde{f}_D, \tau] = \text{IDFT} \left\{ \text{DFT}(r_{\tilde{f}_D}[jN, \dots, jN + N - 1]) \cdot \text{DFT}(s_{\tilde{f}_D}[jN, \dots, jN + N - 1])^* \right\}, \quad (4)$$

where

$$\tau = [0, \dots, N - 1] \quad (5)$$

and where DFT and $IDFT$ are respectively the discrete Fourier transform and the inverse discrete Fourier transform operators. The local code $s_{\tilde{f}_D}$ is generated with a chip rate

$$R_D = R_{chip} \left(1 + \frac{\tilde{f}_D}{f_0} \right), \quad (6)$$

which compensates for the Doppler effect on the PRN code.

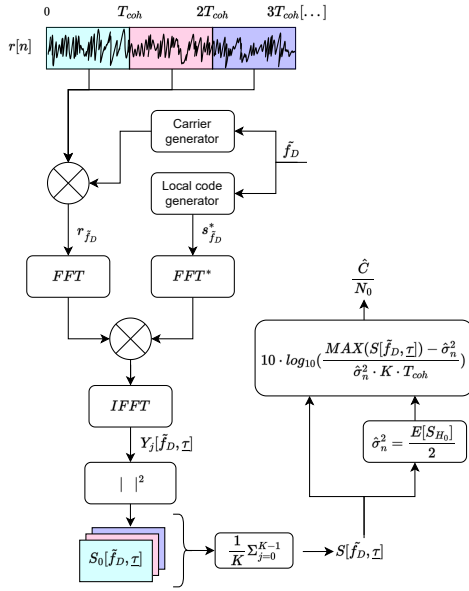


Fig. 3. Schematic representation of the acquisition scheme.

B. Acquisition threshold

Following the evaluation of the CAF, the acquisition is considered successful when the correlation peak exceeds a predefined threshold. By fixing a target system probability of false alarm p_{fa} , the probability of false alarm per cell can be expressed as

$$p_{fa,cell} = 1 - (1 - p_{fa})^{\frac{1}{L}}, \quad (7)$$

where L denotes the size of the search space, i.e., the total number of frequency-offset and code-phase bins. The threshold can then be set to

$$Th = \hat{\sigma}_n^2 \cdot \chi^{-2}(K, p_{fa,cell}), \quad (8)$$

where χ^{-2} is the inverse chi-square function. The term $\hat{\sigma}_n^2$ refers to the estimated noise variance measured at the acquisition stage. To obtain $\hat{\sigma}_n^2$, according to the literature [21], [22], it is possible to consider the correlation under the null hypothesis H_0 in the Neyman-Pearson sense [23] as the portion of CAF S_{H_0} located away from the correlation peak of at least one chip in the code phase domain. The expression of the noise variance estimate $\hat{\sigma}_n^2$ is

$$\hat{\sigma}_n^2 = \frac{E[S_{H_0}]}{2}. \quad (9)$$

For all operations, in this work, the system probability of false alarm is set to 0.001.

C. C/N_0 characterization

Several methods for estimating C/N_0 are available in the literature; some rely on the outputs of the correlators at the tracking stage [24], such as the Moment Method

TABLE III

Acquisition parameters used in post-processing during the acquisition campaign. Underlined values denote the settings adopted for the statistics reported in this work. Signals acquired with the secondary or overlay code are annotated accordingly.

Signal	K non-coh. int.	T_{coh} (ms)	Secondary
GPS C/A	<u>15</u> , 20, 30	<u>4</u> , 8	—
E1B	<u>15</u> , 20, 30, 40	<u>4</u>	—
B1C (Pilot)	<u>5</u> , 10, 15, 20	<u>10</u>	✓
QZSS L1 C/A	<u>15</u> , 20, 30	<u>4</u> , 8	—
NavIC L1 (SPS)	<u>5</u> , 10, 15, 20	<u>10</u>	—
L5Q	<u>20</u>	<u>2</u> , 4, 8	—
E5aI	<u>20</u>	<u>2</u> , 4, 8	—
B2aD (Data)	<u>10</u> , 15, 20, 30, 35	<u>5</u>	✓
QZSS L5I	<u>10</u> , 15, 20, 25	<u>10</u>	✓
NavIC L5	<u>20</u>	4, <u>8</u>	—
SBAS L1	<u>15</u>	<u>4</u>	—
SBAS L5Q	<u>30</u>	<u>1</u>	—

(MM) and Narrow-Wideband Power Ratio (NWPR) approaches. However, given the reduced length of the IQS snapshots, it is relevant to reliably estimate C/N_0 during the acquisition stage, for this purpose, the estimator chosen in this analysis is based on the Non-coherent Post Detection Integration (NPDI) estimator introduced in [22]. The estimate of C/N_0 , in dB-Hz, is obtained as

$$\frac{\hat{C}}{N_0} = 10 \cdot \log_{10} \left(\frac{MAX(S[\tilde{f}_D, \tau]) - \hat{\sigma}_n^2}{\hat{\sigma}_n^2 \cdot K \cdot T_{coh}} \right). \quad (10)$$

This estimator is specifically intended for non-coherent integration and it is shown hereafter that it has a reduced bias in the range of C/N_0 values considered in this work.

To understand how the bias introduced by the estimator affects the measurements, a set of simulations is conducted to evaluate the range in which the estimator is in its unbiased regime. A synthetic GPS L1 C/A signal is generated with a sampling frequency of 8 MHz and a quantization depth of 8 bits. Fifteen C/N_0 values, linearly spaced between 15 and 55 dB-Hz, are tested. For each C/N_0 level, 90 trials with independent noise realizations are evaluated using the estimator defined in (10). The number of non-coherent integrations is set to $K = 15$, with a coherent integration time $T_{coh} = 4$ ms. As shown in Fig. 4, the NPDI based estimator exhibits a bias at higher simulated C/N_0 values, causing the estimated value to negatively diverge from the true one. A similar behavior is also observed at lower C/N_0 levels where estimated values become quickly unreliable as C/N_0 drops below 25 dB-Hz. Taking into account the chosen acquisition parameters and the simulation setup, the estimated C/N_0 range between 25 and approximately 40 dB-Hz are assumed reliable. Given the limited number of non-coherent integrations and the length of the coherent integration times adopted in this work, the C/N_0 values that can be observed considering the receiver sensitivity are expected to fall within this range in most of the tested scenarios.

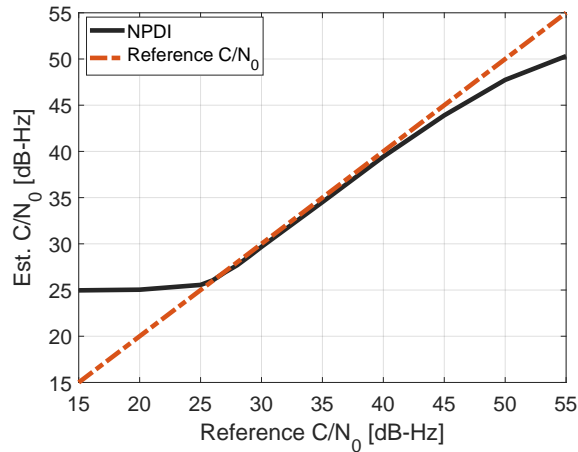


Fig. 4. Comparison between expected and measured C/N_0 . Generated C/N_0 (orange), estimated C/N_0 (black). Coherent integration time T_{coh} : 4 ms, non coherent integrations: K : 15.

To obtain an estimate of C/N_0 from the available dataset, the estimation process is repeated for multiple adjacent and non-overlapping portions of the IQS snapshots and then the results are averaged together to obtain a single C/N_0 estimate.

D. Extended Space Service Volume Simulator

The extended SSV simulator used in this work models the GNSS, RNSS, and SBAS constellations relevant to the analysis. It propagates broadcast ephemerides to determine satellite positions and generates the corresponding observables, including C/N_0 , geometric Doppler shift, and pseudoranges. To estimate satellite visibility and received C/N_0 for L1 C/A and L5 signals at the spacecraft location, the simulator assigns to each satellite an antenna radiation pattern derived from the available literature. Table IV summarizes the pattern adopted for each constellation.

High-fidelity three-dimensional gain patterns are available for GPS, Galileo, and QZSS on both L1 and L5; these are directly incorporated into the simulation. For BeiDou, complete antenna patterns have not yet been published at the time of writing. The simulator therefore employs the Min-Model, which provides a conservative representation of the main lobe for each band [25] and reconstructs the corresponding pattern through interpolation of the published values.

For other RNSS systems, detailed radiation patterns are similarly unavailable. In the case of GPS-Aided GEO Augmented Navigation (GAGAN) and IRNSS, an approximate antenna pattern is derived from CanX-2 mission measurements reported in [11]. This pattern is constructed by interpolating the available points conservatively, preserving the main lobe while assigning low gain at large off-boresight angles. For the remaining SBAS constellations, except for GAGAN, the BeiDou Min-Model is

used for Geostationary Earth Orbit (GEO) and Inclined Geosynchronous Orbit (IGSO) satellites.

To take full advantage of the LuGRE dataset, the link budget for each constellation is calibrated using measurements collected during the mission. For GPS and Galileo, more than 106 hours of RTP observations support a high-accuracy calibration. The procedure begins by assuming nominal transmit power values and running an initial simulation across all relevant operations. The residuals between the simulated and measured C/N_0 values are evaluated considering only the epochs in which the signals from the main lobes of the transmitting satellites are in radiometric visibility. These residuals are then aggregated by Pseudo Random Noise (PRN) and frequency band. The resulting biases, expressed as penalties or gains, are applied to the corresponding satellites to align the simulations with the observed data.

For the remaining GNSS, RNSS, and SBAS constellations, calibration relies exclusively on the C/N_0 estimates obtained from the IQS snapshots collected during SC operations. Although this provides a less accurate calibration, due to the limited number of available measurements and the absence of detailed antenna patterns, it enables, for the first time, a simulation of multi-constellation signal availability in the cis-lunar environment based directly on experimental observations acquired in cis-lunar space and at the lunar surface. It is important to note that the power distribution among the various signal components for GPS, as well as for other constellations, may vary over time, for instance, in the case of GPS, due to the feature called flex power mode [26].

SBAS signals on L5 were excluded due to limited information and for the potentially large variety of L5 antenna patterns. Additionally, some SVs transmit both ranging and augmentation signals, namely BeiDou GEO-1/2/3 and all QZSS satellites except QZS-1. Their ranging signals count toward their constellations, while augmentation signals are treated separately and not counted as SBAS. It can be anticipated that the PRNs acquired are associated to the signals that, according to the simulator outputs, are all coming from the mainlobes of the transmitting satellites and are all expected to be in radiometric visibility.

IV. Results and Analysis

A. Acquisition Results from IQ Snapshots Collected in the Lunar Domain

A comprehensive overview of all successful acquisitions is reported in Table V and in Table VI for L1/E1 and L5/E5a bands, respectively. Although the SC operations were optimized solely for GPS and Galileo visibility, a significant number of signals from the BeiDou RNSS and various SBASs were acquired from the available IQS snapshots. This result is illustrated in Fig. 5(a) and Fig. 5(b), which show, for each SC operation, the number of acquired PRN signals per system and per band as

TABLE IV

Antenna patterns used in the extended SSV simulator for each GNSS, RNSS, and SBAS constellation. Patterns available per SV on L1 or L5 bands are marked accordingly.

Constellation	Per-SV Availability	Description	References
GPS	✓*	Official antenna pattern pre-flight measurements released by Lockheed Martin and Boeing.	[27]
Galileo	—	GRAP model.	[28]
BeiDou (BDS-3)	—	Min-model of the antenna main lobe, available per band and orbit type.	[25] [29]
QZSS	✓	Official antenna pattern released by the Japan Aerospace Exploration Agency (JAXA).	[30]
NavIC (IRNSS)	—	Pattern available only for a submodule of the antenna. The patterns used correspond to BeiDou BDS-3 (B1) GEO-IGSO.	[31]
SBAS	—	Patterns used in the simulations correspond to BeiDou BDS-3 (B1) GEO-IGSO **.	—

* Pattern available for each SV except block IIF (released at block level) and for SVs with PRN 1, 11, 21, and 28, which are not available.

** Except for GAGAN [11].

a function of the spacecraft altitude at the start of the operation, expressed in Earth Radii (RE). Among all operations, OP38_0 did not yield any successful acquisitions. In contrast, the snapshot associated with OP78_1, despite being collected at a high altitude, produced the highest number of L1 acquisitions, while OP9_0 resulted in the largest number of L5 acquisitions.

Fig. 6(a) and Fig. 6(b) present the distribution of C/N_0 values for each signal on the L1 and L5 bands, together with the number of successful acquisitions per signal. The analysis indicates that expanding the set of processed signals to include those of additional GNSS, RNSS, and SBAS constellations substantially increases the total number of successful acquisitions. On the L1 band, the largest contributions arise from SBAS and BeiDou, whereas on the L5 band, BeiDou and IRNSS are the most significant. Notably, the NavIC L5 signal is characterized by a chip rate of 1.023 Mchip/s, which is 10 times lower than the chip rate of all other L5 signals, making it uniquely oversampled. It is worth recalling that all L5 SC operations were instead performed at a nominal sampling rate of 24 MHz.

B. Simulated Signal Availability

The acquisitions performed on the IQS snapshots from LuGRE were used to tune the extended SSV simulator by adjusting the transmitted power of each constellation. This section presents the simulation results corresponding to the scenarios encountered by BGM1 during the LuGRE operational windows.

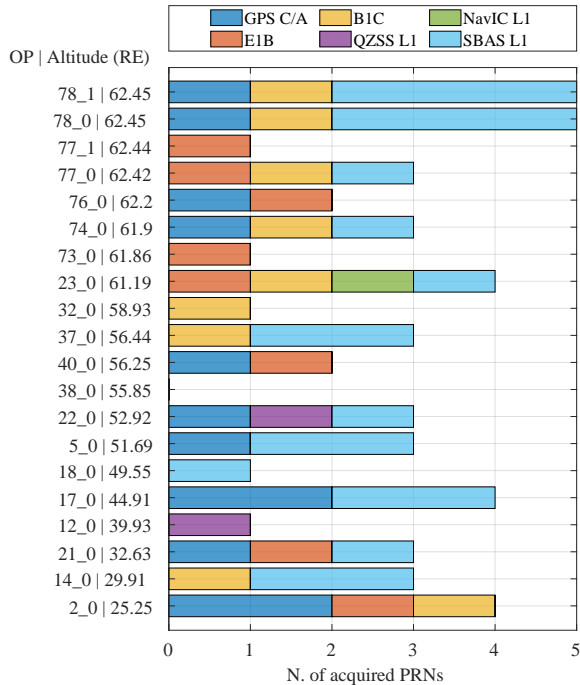
For all subsequent analyses, a threshold of 26 dB-Hz is used. This value provides a conservative margin, since the LuGRE receiver has successfully tracked signals with an estimated C/N_0 of about 24 dB-Hz [2]. The selected threshold also improves robustness against possible modeling inaccuracies and other sources of signal degradation.

It is important to note that the results shown here, besides the selected sensitivity threshold, are receiver-agnostic; different receivers may adopt different acquisition and tracking strategies, and their effective thresholds can vary depending on both environmental conditions and internal receiver state.

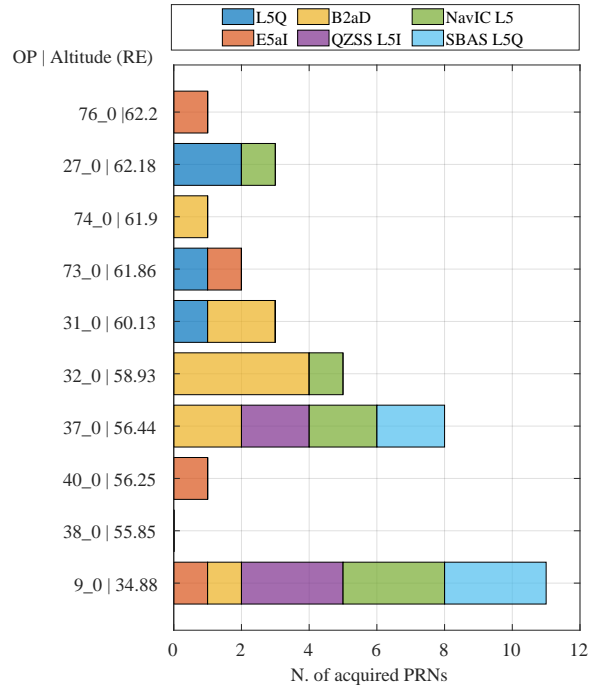
Fig. 7(a) and Fig. 7(b) illustrate the percentage of the nominal RTP operation duration during which n signals from n distinct satellites exceed the selected C/N_0 threshold. Specifically, Fig. 7(a) presents the multi-frequency, multi-constellation scenario including only GPS and Galileo, while Fig. 7(b) shows the case where additional GNSS, RNSS, and SBAS constellations are also considered. The figures show an increase in the availability introduced by the additional constellations; however, some operations are still characterized by a reduced number of satellites in radiometric visibility, such as the case of OP74_0 and OP27_0. Including BeiDou, as well as the RNSS and SBAS constellations, increases the percentage of epochs with at least four satellites in radiometric visibility from 11.7% to 46.1%. The adopted threshold, i.e., $n \geq 4$, was considered as it represents the minimum requirement for autonomous receiver state estimation, assuming the use of limited a priori information to guarantee solution convergence (e.g. through a Least-Squares estimation). This condition allows for the reliable initialization of more advanced orbit determination filters such as Bayesian estimation filters devoted to Precise orbit determination (POD).

C. Dilution of precision

A partial reduction in Geometric Dilution Of Precision (GDOP) resulting from the inclusion of additional constellations can be observed in Fig. 8, which shows the GDOP values for all the operations in which the evaluation was possible. As it can be noticed, a wide



(a) L1 band



(b) L5 band

Fig. 5. Number of acquired signals for each operation. Operations are ordered as function of altitude expressed in RE.

range of GDOP values is observed, reaching a maximum at almost 10,000 and a minimum close to 300. During some operations, including SBAS and RNSS satellites in the set of satellites used for GDOP computation leads to an improvement in GDOP. This effect is particularly evident in operations OP17_0, OP23_0, OP37_0, OP38_0 and OP76_0. When GDOP cannot be evaluated without SBAS or RNSS satellites, the contribution to the availability increase becomes evident. Fig. 9 illustrates a distinctive operational condition, showing the C/N_0 values generated by the extended SSV simulator. During OP38_0, the Galileo E1B signal exhibits a consistent pattern, as reported in [2]; signals from SVs on orbital plane B progressively fade, while those on plane A remain visible with higher C/N_0 despite increasingly prolonged Earth-shadowing periods. The simulations also show that the Medium Earth Orbit (MEO) SVs of the BeiDou constellation follow a similar fading pattern, whereas the BeiDou IGSO and GEO satellites do not. This naturally mitigates the unfortunate phasing phenomena at lunar surface. However, it is important to remark that the use of SBAS signals for ranging purposes may require more accurate ephemerides and additional corrections with respect to those broadcast by the SVs themselves [11].

V. Conclusions

This work highlights the scientific value of the LuGRE IQS snapshots for assessing satellite navigation and augmentation systems signal availability in the lunar and cis-lunar environments independently from actual real-

time operation of the LuGRE payload. Despite significant frequency drift, reduced sampling rates, coarse (4-bit) quantization, and very short snapshot durations, the experimental data demonstrated that signals can be acquired using relatively simple acquisition techniques.

The experimental results are used to calibrate the extended SSV simulator. The simulation of mission operations shows that extending the analysis beyond GPS and Galileo to include BeiDou, regional navigation satellite systems such as IRNSS (NavIC) and QZSS, as well as SBAS constellations, leads to a significant improvement in signal availability. In particular, in a dual-frequency multi-constellation configuration, the percentage of total epochs in which at least four satellites are in radiometric visibility increases from 11% to 46% with respect to the GPS- and Galileo-only case. Nevertheless, despite this improvement, there remain mission phases in which fewer than four satellites are simultaneously in radiometric visibility. In addition to improving availability, processing multiple constellations increases the probability of meeting the minimum visibility required for a-priori-free convergent navigation solutions, allowing on-demand filter initialization without long delays, although high-sensitivity acquisition may still be required. The inclusion of RNSS and SBAS GEO constellations further enhances orbital geometry diversity, mitigating geometry-dependent effects such as orbital-plane-related signal fading observed during specific operational periods (e.g., OP38_0), and thereby improving availability, at the cost of requiring additional corrections for the SBAS SVs [11].

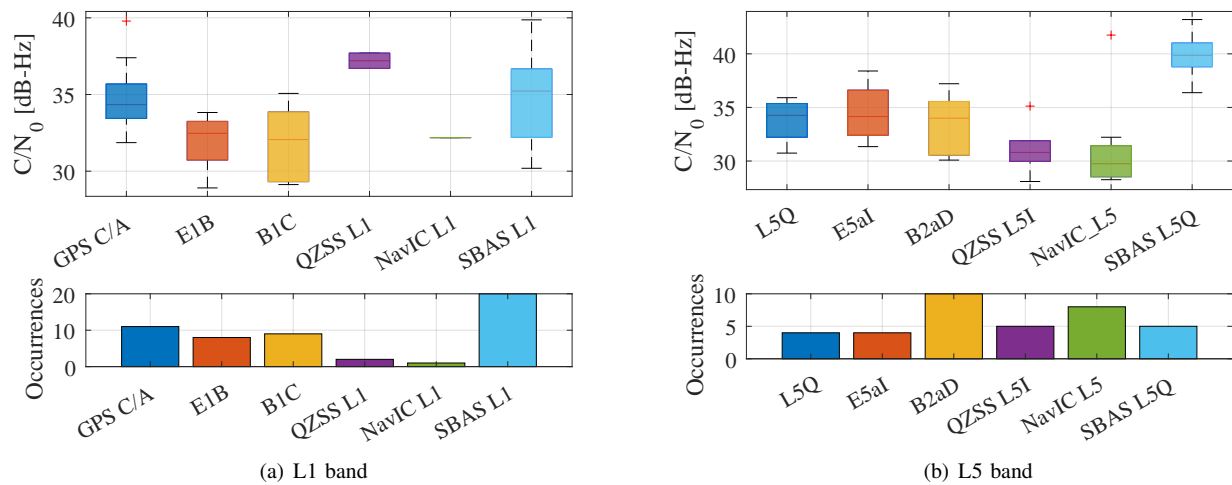
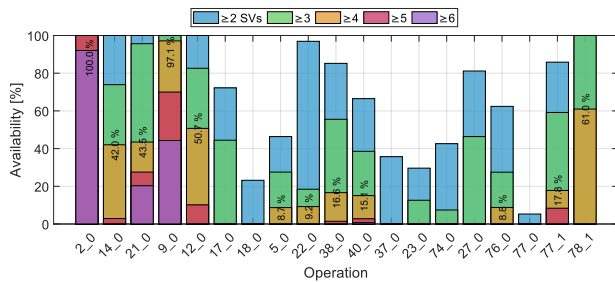
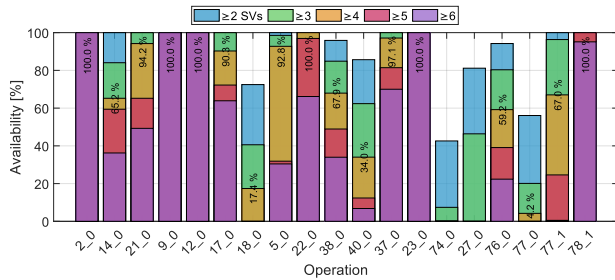


Fig. 6. Distribution of the carrier-to-noise density ratio (C/N_0) for different GNSS signals in the L1 and L5 bands. For each signal, the central line of the box represents the median C/N_0 , the box spans the interquartile range (25th–75th percentiles), and the whiskers extend to the most extreme values excluding outliers. Outliers, when present, are indicated by individual markers. The lower panel reports the number of occurrences for each signal.



(a) GPS + Galileo



(b) GNSS + RNSS + SBAS

Fig. 7. Multi-constellation, multi-frequency availability as the percentage of nominal RTP operation with n signals from n distinct GNSS satellites above the C/N_0 threshold. Percentages are shown for $n \geq 4$.

Overall, the presented results motivate further research on robust high-sensitivity acquisition, frequency-drift compensation, and multi-constellation navigation architectures for future lunar missions. In addition, they highlight the need for more accurate antenna radiation pattern modeling to enhance simulation fidelity, particularly for BeiDou and the RNSS and SBAS constellations.

Acknowledgment

This study was funded within the contract n. 2021-26-HH.0 between Agenzia Spaziale Italiana and Politecnico di Torino "Attività di Ricerca e Sviluppo inerente alla Navigazione GNSS nello Space volume Terra/Luna nell'ambito del Lunar GNSS Receiver Experiment".

This publication is also part of the project PNRR-NGEU which has received funding from the MUR – DM 630/2024.

REFERENCES

- [1] SpaceNews, "Novaspaces forecasts global space exploration investment to reach \$31 billion by 2034," Apr. 2025. Accessed: 2025-12-22.
- [2] J. J. K. Parker, F. Dovis, L. Konitzer, N. Esantsi, B. Ashman, A. Minetto, A. Nardin, O. Vouch, S. Zocca, F. Bernardi, M. Boschiero, S. Fantinato, E. Miotti, C. Facchinetti, M. Musmeci, and G. Varacalli, "GNSS Reception at the Moon: First Results of the Lunar GNSS Receiver Experiment (LuGRE) [Under Review]," *Navigation: Journal of the Institute of Navigation*, 2025.
- [3] J. J. Parker, F. Dovis, B. Anderson, L. Ansalone, B. Ashman, F. H. Bauer, G. D'amore, C. Facchinetti, S. Fantinato, G. Impresario, *et al.*, "The lunar GNSS receiver experiment (LuGRE)," in *Proceedings of the 2022 International Technical Meeting of The Institute of Navigation*, pp. 420–437, 2022.
- [4] L. Konitzer, J. J. Parker, B. Ashman, N. Esantsi, C. Facchinetti, F. Dovis, A. Minetto, A. Nardin, F. Bauer, L. Ansalone, *et al.*, "Science objectives and investigations for the lunar GNSS receiver experiment (LuGRE)," in *Proceedings of the 37th International Technical Meeting of the Satellite Division of The Institute of Navigation (ION GNSS+ 2024)*, pp. 1061–1081, 2024.
- [5] S. Tedesco, F. Bernardi, S. Guzzi, M. Boschiero, M. Pulliero, D. Marcantonio, M. Ghedin, E. Miotti, S. Fantinato, O. Pozzobon, *et al.*, "Deep space GNSS in moon transfer orbit: the LuGRE receiver," in *2023 IEEE International Conference on Wireless for Space and Extreme Environments (WiSEE)*, pp. 1–6, IEEE, 2023.

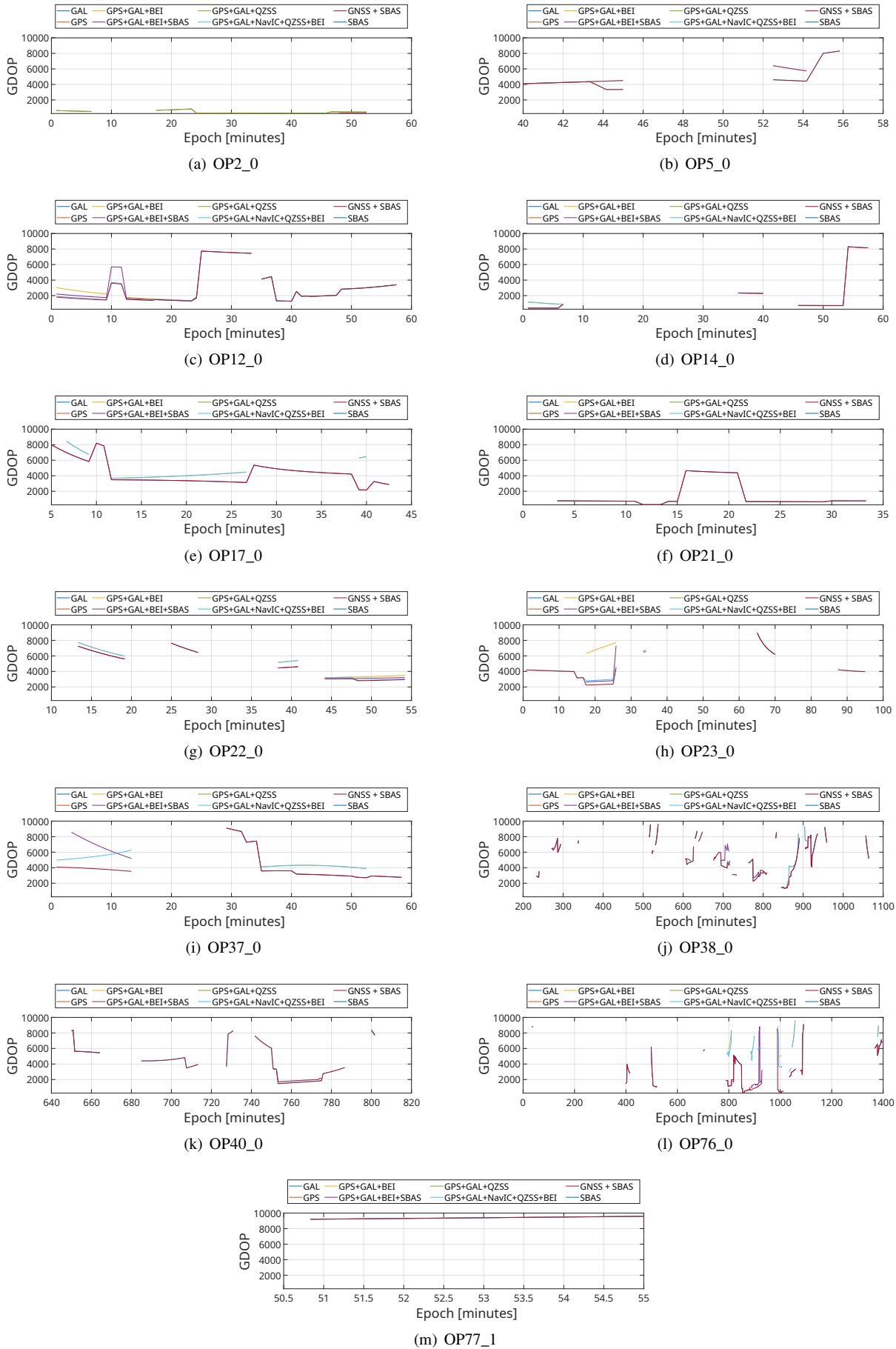


Fig. 8. GDOP values corresponding to the set of operations where evaluation was possible.

TABLE V

List of the signals acquired on L1 band.

*PRN below the threshold but present on L5,
predicted to be close to the radio visibility threshold and with a
correlation peak distinguishable from the noise floor.

Excluded from the statistics.

Operation	Signal	PRN	C/N ₀ [dB-Hz]
Commissioning and Transit			
OP2_0	GPS C/A	18	39.7
	GPS C/A	24	37.4
	E1B	36	33.8
	B1C	34	33.6
OP5_0	GPS C/A	28	34.6
	SBAS L1 - BDSBAS	130	30.6
	SBAS L1 - SouthPAN	122	34
OP12_0	QZSS L1	3	36
OP14_0	B1C	36	35
	SBAS L1 - WAAS	133	37
	SBAS L1 - WAAS	135	36.8
OP17_0	GPS C/A	11	34.3
	GPS C/A	30	31.8
	SBAS L1 - BDSBAS	144	35.8
	SBAS L1 - KASS	134	30.1
	SBAS L1 - WAAS	131	34.2
OP21_0	GPS C/A	24	35.8
	SBAS L1 - WAAS	131	39.8
	E1B	11	32.4
OP22_0	GPS C/A	31	34
	QZSS L1	3	37.7
	SBAS L1 - MSAS	137	30.9
Lunar Orbit			
OP23_0	B1C	39	33
	E1B	33	32.2
	NavIC L1	10	32.2
	SBAS L1 - BDSBAS	130	32.4
OP32_0	B1C	34	34.2
	B1C	50*	-
OP37_0	B1C	39	29.1
	QZSS L1	3*	-
	QZSS L1	7*	-
	SBAS L1 - BDSBAS	143	37.3
	SBAS L1 - MSAS	137	32
Lunar Surface			
OP40_0	GPS C/A	25	31.1
	E1B	31	31.3
OP73_0	E1B	33	32.7
OP74_0	B1C	26	30.8
	GPS C/A	31	33.2
	SBAS L1 - EGNOS	136	35
OP76_0	GPS C/A	31	32.2
	E1B	26	30.3
OP77_0	B1C	45	29.3
	E1B	13	32.6
	SBAS L1 - AL-SBAS	148	31.3
OP77_1	E1B	33	28.9
OP78_0	B1C	37	29.2
	GPS C/A	12	34.1
	SBAS L1 - WAAS	131	38.8
	SBAS L1 - WAAS	133	33.8
	SBAS L1 - WAAS	135	36.5
OP78_1	B1C	37	32
	GPS C/A	12	35
	SBAS L1 - WAAS	131	35.3
	SBAS L1 - WAAS	133	36
	SBAS L1 - WAAS	135	35.3

TABLE VI

List of the signals acquired on L5 band.

Operation	Signal	PRN	C/N ₀ [dB-Hz]
Commissioning and Transit			
OP9_0	E5aI	26	38.8
	B2aD	34	34.1
	QZSS L5I	3	30.8
	QZSS L5I	4	30.5
	QZSS L5I	7	35.1
	NavIC L5	4	28.5
	NavIC L5	5	32.2
	NavIC L5	7	41.7
	SBAS L5Q - BDSBAS	130	43.2
	SBAS L5Q - QZSS	185	39.6
	SBAS L5Q - QZSS	186	39.8
Lunar Orbit			
OP27_0	L5Q	23	34.8
	L5Q	26	33.7
	NavIC L5	6	30.7
OP31_0	L5Q	23	35.9
	B2aD	29	33.9
	B2aD	48	35.5
OP32_0	B2aD	34	37
	B2aD	50	32.9
	B2aD	40	30.7
	B2aD	43	29.8
	NavIC L5	5	28.8
OP37_0	B2aD	39	36.4
	B2aD	44	30.4
	QZSS L5I	7	30.8
	QZSS L5I	3	28
	NavIC L5	5	28.8
	NavIC L5	10	29.2
	SBAS L5Q - BDSBAS	143	40.2
SBAS L5Q - QZSS	185	36.4	
Lunar Surface			
OP40_0	E5aI	31	33.4
OP73_0	L5Q	24	30.7
	E5aI	33	34.8
OP74_0	B2aD	26	34.9
OP76_0	E5aI	26	31.3

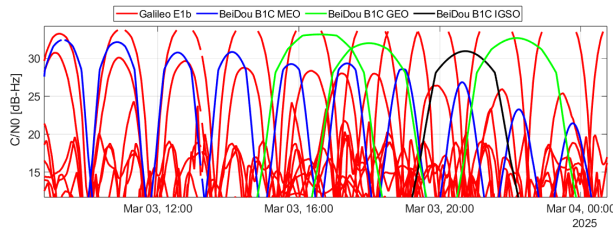


Fig. 9. Sample of simulated C/N_0 trends associated to a portion of OP38_0.

- [6] M. Pulliero, G. Cittadin, M. Boschiero, M. Ghedin, D. Marcantonio, S. Fantinato, E. Miotti, O. Pozzobon, C. Facchinetti, M. Musmeci, *et al.*, "The Space Qualification Process of the LuGRE GNSS Payload," in *2023 IEEE International Conference on Wireless for Space and Extreme Environments (WiSEE)*, pp. 7–12, IEEE, 2023.
- [7] J. Parker, F. Dovis, O. Pozzobon, C. Facchinetti, B. Anderson, B. Ashman, F. H. Bauer, F. Bernardi, M. Boschiero, G. Campagnolo, S. Fantinato, F. Fiorina, M. Ghedin, S. Guzzi, C. Heighes, L. Konitzer, D. Martini, S. McKim, J. J. Miller, A. Minetto, E. Miotti, N. Montini, L. Morichi, M. Musmeci, A. Nardin, M. Pulliero, S. Sanathanamurthy, L. Sciacca, S. Tedesco, L. Valencia, G. Varacalli, O. Vouch, and S. Zocca, "Lunar GNSS Receiver Experiment (LuGRE) Mission Data." <https://zenodo.org/doi/10.5281/zenodo.16411687>, 2025.
- [8] L. B. Winternitz, W. A. Bamford, S. R. Price, J. R. Carpenter, A. C. Long, and M. Farahmand, "Global Positioning System Navigation Above 76,000 km for NASA's Magnetospheric Multiscale Mission," *NAVIGATION*, vol. 64, no. 2, pp. 289–300, 2017.
- [9] L. B. Winternitz, W. A. Bamford, and S. R. Price, "New high-altitude GPS navigation results from the magnetospheric multiscale spacecraft and simulations at Lunar distances," in *Proceedings of the 30th International Technical Meeting of The Satellite Division of the Institute of Navigation (ION GNSS+ 2017)*, pp. 1114–1126, 2017.
- [10] D. Baird, "Record-breaking satellite advances NASA's exploration of high-altitude GPS," www.nasa.gov, 2019. Accessed on: Nov. 23, 2022.
- [11] E. Kahr, O. Montenbruck, and K. O'Keefe, "An analysis of SBAS signal reception in space," *Navigation: Journal of The Institute of Navigation*, vol. 63, no. 3, pp. 321–333, 2016.
- [12] K. Sarda, C. Grant, S. Eagleson, D. D. Kekez, and R. E. Zee, "Canadian Advanced Nanospace Experiment 2 orbit operations: two years of pushing the nanosatellite performance envelope," in *ESA small satellites, services and systems symposium*, vol. 20, 2010.
- [13] A. Nardin, A. Minetto, S. Guzzi, F. Dovis, L. Konitzer, and J. J. K. Parker, "Snapshot tracking of GNSS signals in space: A case study at lunar distances," in *Proceedings of the 36th International Technical Meeting of the Satellite Division of The Institute of Navigation (ION GNSS+ 2023)*, (Denver, Colorado), pp. 3267–3281, September 2023.
- [14] A. Nardin, A. Minetto, O. Vouch, M. Mariani, and F. Dovis, "Snapshot acquisition of GNSS signals in space: a case study at lunar distances," in *Proceedings of the 35th International Technical Meeting of the Satellite Division of The Institute of Navigation (ION GNSS+ 2022)*, (Denver, Colorado), pp. 3603 – 3617, September 2022.
- [15] E. Kaplan and C. Hegarty, *Understanding GPS/GNSS: Principles and Applications*. Artech House, 2017.
- [16] D. Van Nee and A. Coenen, "New fast GPS code-acquisition technique using FFT," *Electronics Letters*, vol. 27, no. 2, pp. 158–160, 1991.
- [17] J. B.-Y. Tsui, *Fundamentals of global positioning system receivers: a software approach*. John Wiley & Sons, 2004.
- [18] D. Borio, *A statistical theory for GNSS signal acquisition*. PhD thesis, Politecnico di Torino, 2008.
- [19] M. Foucras, O. Julien, C. Macabiau, and B. Ekambi, "Detailed analysis of the impact of the code Doppler on the acquisition performance of new GNSS signals," in *Proceedings of the 2014 International Technical Meeting of The Institute of Navigation*, pp. 513–524, 2014.
- [20] L. Sciacca, A. Minetto, A. Nardin, S. Tedesco, M. Boschiero, S. Fantinato, L. Canzian, and F. Dovis, "Acquiring GNSS Signals in Cislunar Space: A Hardware-in-the-Loop Investigation for LuGRE Mission Data," in *2025 IEEE/ION Position, Location and Navigation Symposium (PLANS)*, pp. 1036–1045, IEEE, 2025.
- [21] J. W. Betz, "Effect of partial-band interference on receiver estimation of C/N_0 ," in *Proceedings of the 2001 National Technical Meeting of the Institute of Navigation*, pp. 817–828, 2001.
- [22] D. Gómez-Casco, J. A. López-Salcedo, and G. Seco-Granados, "C/N0 estimators for high-sensitivity snapshot GNSS receivers," *GPS Solutions*, vol. 22, no. 4, p. 122, 2018.
- [23] J. Neyman and E. S. Pearson, "On the problem of the most efficient tests of statistical hypotheses," *Philosophical Transactions of the Royal Society of London. Series A, Containing Papers of a Mathematical or Physical Character*, vol. 231, no. 694–706, pp. 289–337, 1933.
- [24] M. Pini, E. Falletti, and M. Fantino, "Performance evaluation of C/N0 estimators using a real time GNSS software receiver," in *2008 IEEE 10th international symposium on spread spectrum techniques and applications*, pp. 32–36, IEEE, 2008.
- [25] C. Xinuo and Z. Jinjun, "BDS Space Service Volume SSV Performance and Applications." https://www.unoosa.org/documents/pdf/icg/2023/ICG-17/icg17_wgb_07.pdf, 2023. Accessed: 2025-11.
- [26] P. Steigenberger, S. Thörlert, and O. Montenbruck, "Flex power on GPS block IIR-M and IIF," *GPS solutions*, vol. 23, no. 1, p. 8, 2019.
- [27] US Navigation Center, "GPS Technical References." <https://www.navcen.uscg.gov/gps-technical-references>, 2025. Accessed: 2025-11-10.
- [28] F. Menziona, M. Sgammini, M. Paonni, *et al.*, "Reconstruction of Galileo Constellation Antenna Pattern for Space Service Volume Applications," *Publications Office of the European Union*, 2024.
- [29] K. Lin, X. Zhan, R. Yang, F. Shao, and J. Huang, "BDS Space Service Volume characterizations considering side-lobe signals and 3D antenna pattern," *Aerospace Science and Technology*, vol. 106, p. 106071, 2020.
- [30] JAXA, "QZSS Antenna Patterns." <https://qzss.go.jp/en/technical/antenna-patterns.html>, 2025. Accessed: 2025-11-10.
- [31] R. Jyoti, Sanandiyaa, and e. a. Kumar, H. C. Sanandiyaa, "Wideband Printed Helix Array Antenna at L1 & L5 for Navigation Satellite," in *Proceedings of the International Conference on Antenna Technologies ICAT*, 2005.



Lorenzo Sciacca (Graduate Student Member, IEEE) received his M.Sc. in Communications and Computer Network Engineering from Politecnico di Torino, Italy, in 2024. He is currently pursuing a Ph.D. at the Department of Electronics and Telecommunications, Politecnico di Torino, as part of the Navigation Signal Analysis and Simulation (NavSAS) group. His research focuses on developing high-sensitivity, environment-aware GNSS receivers to improve navigation in challenging conditions, including lunar and cis-lunar

environments. He has been involved in the Lunar GNSS Receiver Experiment (LuGRE) since 2025.



Alex Minetto (Member, IEEE) received the B.Sc. (2013), M.Sc. (2015), and Ph.D. with honors (2020) in telecommunications and electrical engineering from Politecnico di Torino, where he is now Assistant Professor in the Department of Electronics and Telecommunications and a member of the NavSAS research group. His work focuses on advanced GNSS signal analysis, receiver design, and Bayesian state estimation. He has contributed to ESA and

EUSPA projects and since 2021 has been involved in the Lunar GNSS Receiver Experiment (LuGRE) as a mission's Science Team member.



Andrea Nardin (Member, IEEE) received the M.Sc. (2018) and Ph.D. with honors (2023) in telecommunications and electrical engineering from Politecnico di Torino, where he is now Assistant Professor in the Department of Electronics and Telecommunications and a member of the NavSAS research group. In 2021, he was a Visiting Doctoral Researcher at Northeastern University, Boston. His research interests include signal processing architectures and signal

design for GNSS and next-generation PNT systems.



Fabio Dovis (Member, IEEE) received the M.Sc. (1996) and Ph.D. (2000) from Politecnico di Torino, where he is now Full Professor in the Department of Electronics and Telecommunications and coordinator of the NavSAS Research Group. His research focuses on GNSS receiver design, advanced signal processing for interference and multipath mitigation, and ionospheric monitoring. He has extensive experience in international projects,

collaborations with industry and research institutions, and serves on the IEEE AESS Navigation Systems Panel.



Luca Canzian joined Qascom in 2015 and he is currently leading the R&D domain area. He has worked in several projects with ESA, ASI, NASA, the European Commission and Industry. His main expertise involves ground-based and space-based location systems, detection and location of interference signals, navigation using signals of opportunity, lunar navigation, inertial navigation systems, orbit determination techniques, GNSS authentication

and anti-spoofing techniques. He holds a MSc degree and a PhD in Electrical Engineering from University of Padova (Italy).



Mario Musmeci received a degree in physics from the University of Rome "La Sapienza." He has worked with major Italian space companies, ESA, and the European Commission on the Galileo program, and co-founded a start-up exploiting a patent based on Galileo signals for reliable traceability of "Made in Italy" products. Since 2016, he has been with ASI's Programs Directorate, serving as technical man-

ager for LuGRE on NASA's Firefly Blue Ghost mission, demonstrating GNSS reception on the lunar surface.



Claudia Facchinetti is a researcher and technologist at the Italian Space Agency (ASI), specializing in Earth observation and space navigation technologies. She holds a Ph.D. in Space Science and Technology and has contributed to numerous scientific projects and space missions, including studies on SAR radar and hyperspectral sensors. She is a key member of the LuGRE (Lunar GNSS Receiver Experiment) team, a joint NASA-ASI initiative

that successfully demonstrated GNSS-based navigation on the Moon during the Firefly Blue Ghost Mission 1 in 2025. Additionally, she is responsible for developing Earth observation missions at ASI.



Giancarlo Varacalli received the degree in Electronic Engineering and holds a Master's degree in Space Systems Engineering from Delft University of Technology. He is currently Head of the Telecommunications and Navigation Department at the Italian Space Agency (ASI). He has held several technical and managerial positions within ASI and serves as Italy's delegate to ESA programme boards in satellite communications and navigation. His

professional interests include satellite telecommunications, navigation systems, and space system engineering.